Proceedings World Geothermal Congress 2023
Beijing, China, April 17 – 21, 2023

Analysis and 1D Joint Inversion of MT and TEM Resistivity Data from Buranga Geothermal Field, Uganda.

Fred Ssemuyaba[1], Knútur Árnason[2], Gylfi Páll Hersir[3], Ásdís Benediktsdóttir[2]

1. Ministry of Energy and Mineral Development, Directorate of Geological Survey and Mines. P.O Box 9 Entebbe, Uganda.

2. Iceland GeoSurvey, ÍSOR Urðarhvarf 8, IS-203 Kópavogur, Iceland

3. Formerly at Iceland GeoSurvey, ÍSOR - presently gylfi.pall@outlook.com

frss@grogtp.is, fredwilkins2@gmail.com

Keywords: *Joint Inversion, Static shift, Resistivity Structure, Fault controlled, amagmatic*

ABSTRACT

Buranga geothermal prospect is the most promising geothermal area within the western branch of the East African Rift System (EARS). Located at the north-eastern base of the Rwenzori mountains and approximately 50km southwest of Fort portal town in Uganda, Buranga is a deep circulation amagmatic system with resistivity structure controlled by NE SW trending deep-seated faults of the Albertine graben which form a border between the Buranga (Semliki) flood plain and the Rwenzori massif.

This paper highlights the key findings of 1D joint inversion of Magneto telluric (MT) and Transient ElectroMagnetic (TEM) data from the area. Data analysis and 1D joint inversion results indicate that the geoelectric strike is in the NE SW direction parallel to the main bounding Bwamba fault and with minor static shifts, mostly away from the soggy sediments.

Results from 1D joint inversion indicate a low resistivity in the sediments due to salinity of the geothermal fluids and/or geothermal alteration in the middle of the prospect area at the border of the sedimentary basin and the Rwenzori massif. This conductive zone extends to a depth close to 5km b.s.l, which is close to the depth to the basement that has been estimated at 5000m b.s.l by oil and gas exploration drilling in the vicinity of the prospect.

1. INTRODUCTION

Over the recent past, the Ministry of Energy and Mineral Development of Uganda, through the Geothermal Resources Department (GRD) embarked on the search for alternative energy sources owing to the ever-increasing demand for clean renewable and sustainable energy resources to drive the growing economy in the different sectors. One of the energy resources that has been earmarked for exploitation is the geothermal energy resource.

Geothermal prospects in Uganda are located within the western branch of the East African rift system (EARS) in the Albertine Graben and are mostly fault-controlled deep circulation systems (Kahwa et al., 2020). This makes these areas somewhat special cases compared to conventional high temperature volcanic-hosted geothermal fields that are found in the Eastern branch of the EARS and other parts of the world. Owing to the uniqueness of the prospects in Uganda, GRD has adapted a site-specific approach of exploration focusing on acquiring geoscientific data and integrating the results in conceptual models directed at targeting geothermal reservoirs heated by deep circulation, like those typical of the United States Basin and Range as well as Western Turkey (Heath et al., 2018). This site-specific exploration approach is aimed at reducing the upfront risks associated with drilling.

In addition to structural geological mapping campaigns and geochemical surveys, Magneto Telluric (MT) and Transient ElectroMagnetic (TEM) resistivity surveys have been undertaken at Buranga (also referred to as Sempaya) to help investigate the characteristics of the resistivity structure in the area to allow for proper delineation of exploitable geothermal reservoir boundaries as well as establishing the potential resource size. Resistivity surveys at Buranga are intended to characterize fault offset of low resistivity sediments and high resistivity Precambrian rocks and detect low resistivity clay caps over possible high resistivity aquifers in the sediments.

The MT method has been used successfully to detect and characterize geothermal areas located in similar extensional tectonics where faults and fractures play a significant role in the deep circulation of geothermal fluids and heat transfer from deep to shallow crustal levels (Faulds et al., 2009 in Kahwa et al., 2020).

2. LOCATION

The Buranga geothermal field is located within the Albertine graben that forms a part of the western branch of the East African Rift System (Figure 1). It runs along the joint border of Uganda and the Democratic Republic of Congo (DRC). The Buranga geothermal field is in Kasitu sub-county in Bwamba county of Bundibugyo district (Nyaketcho, 2008; Sempaya geologic map sheet 56/1,). It is 50 km southwest of Fort Portal town on Bundibugyo Road.

The prospect area is in the Semliki Kaiso sedimentary basin some 300 to 600 m to the northwest of the Bwamba escarpment which forms the NW boundary of the Rwenzori Massif. The Bwamba fault, strikes 20-40° to the northeast and has a dip of 60-65° to the

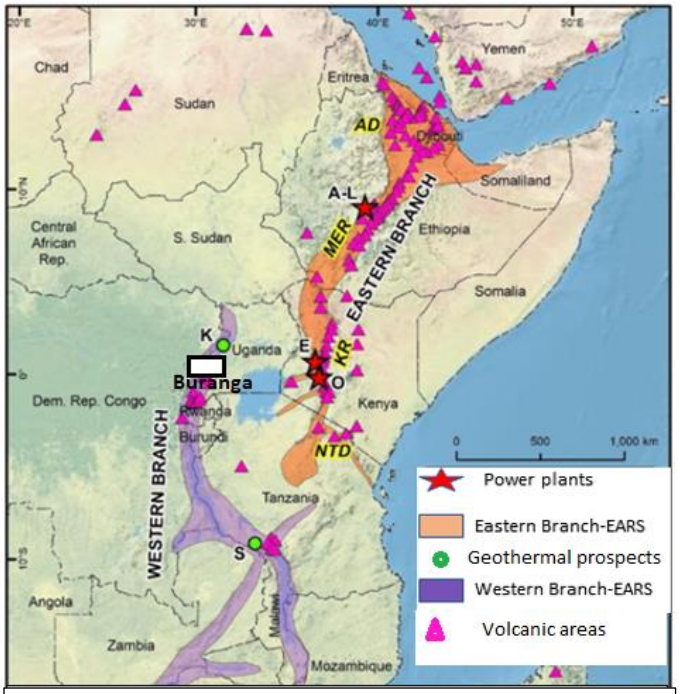

FIGURE 1: Map of the EARS with purple highlighting the Western branch while orange highlights the Eastern branch. (Hinz et al., 2016)

west. The sedimentary basin around Buranga is generally covered with boulder beds and scree. The geothermal activity is found in an area of swamps and rain forest. Surface manifestations cover an area of about 0.12 km^2 and consists of three main hot spring areas: The Mumbuga springs, the Nyansimbe pool and the Kagoro springs. These three groups of springs lay approximately on a line extending some 550 m along a strike N-35°-E, approximately parallel to the Bwamba fault. In addition, springs are found in an area extending some 350m SE of the Nyansimbe pool.

2.1 Regional and Local geology

Uganda is made up of an exposed pre-Cambrian basement dissected by the Western branch of the East African Rift System in the western part of the country. The Western branch, the Albertine Rift, starts in the north at the Sudan border, and curves to the west and then southwest along the border with the Democratic Republic of Congo, and south to Rwanda, Burundi, and western Tanzania.

Spreading in the EARS began over 15 million years ago in Miocene time (EDICON, 1984 in Natukunda, 2010). The western Rift is younger (late Miocene-Recent) than the more mature eastern branch (Morley and Westcott, 1999). The Albertine rift is seismically active, characterized by deep-seated (27- 40 km) large earthquakes (Lindenfeld et al., 2012). The region of the Rift has a markedly higher heat flow than the surrounding Pre-Cambrian terrain. Two different echelon strands are found in the Western Rift Valley, separated by the Rwenzori Mountains, which rise from a base of less than 1,000 m a.s.l in the rift to over 5,000 m a.s.l. Within the Rift Valley, there are thick layers of late Tertiary and Quaternary sediments, freshwater, and saline lakes. Volcanic and plutonic bodies have been identified beneath L. Albert and L. Edward in the south (EDICON, 1984 in Natukunda, 2010).

The Buranga geothermal area is located at the north-western base of the Rwenzori Mountains. A tertiary succession of sands, clays and boulder beds with occasional tuffs have been noted from exploration drilling data. Geological logs from boreholes at Buranga indicate that the Tertiary succession is terminated in the main Bwamba fault zone by a breccia cemented by calc tuff followed by mylonite (Harris et al., 1956 in Natukunda, 2010).

According to Natukunda (2010), the clays are of various colors and the sands are fine-to medium-grained, varying in color between white, brown, grey, and green. The most common binding material is clay, although this may be patchily replaced by calcium carbonate, giving rise to calcareous sandstones and grits.

3. METHODOLOGY

In this study, emphasis has been put on the resistivity methods (MT and TEM). They are commonly found to be the most powerful geophysical methods in geothermal owing to their capability to detect resistivity anomalies related to geothermal activity in the

subsurface. Resistivity is related to key geothermal parameters such as pore structure, water saturation, salinity, alteration minerals and temperature (see e.g., Hersir and Árnason, 2009; Hersir et al., 2022).

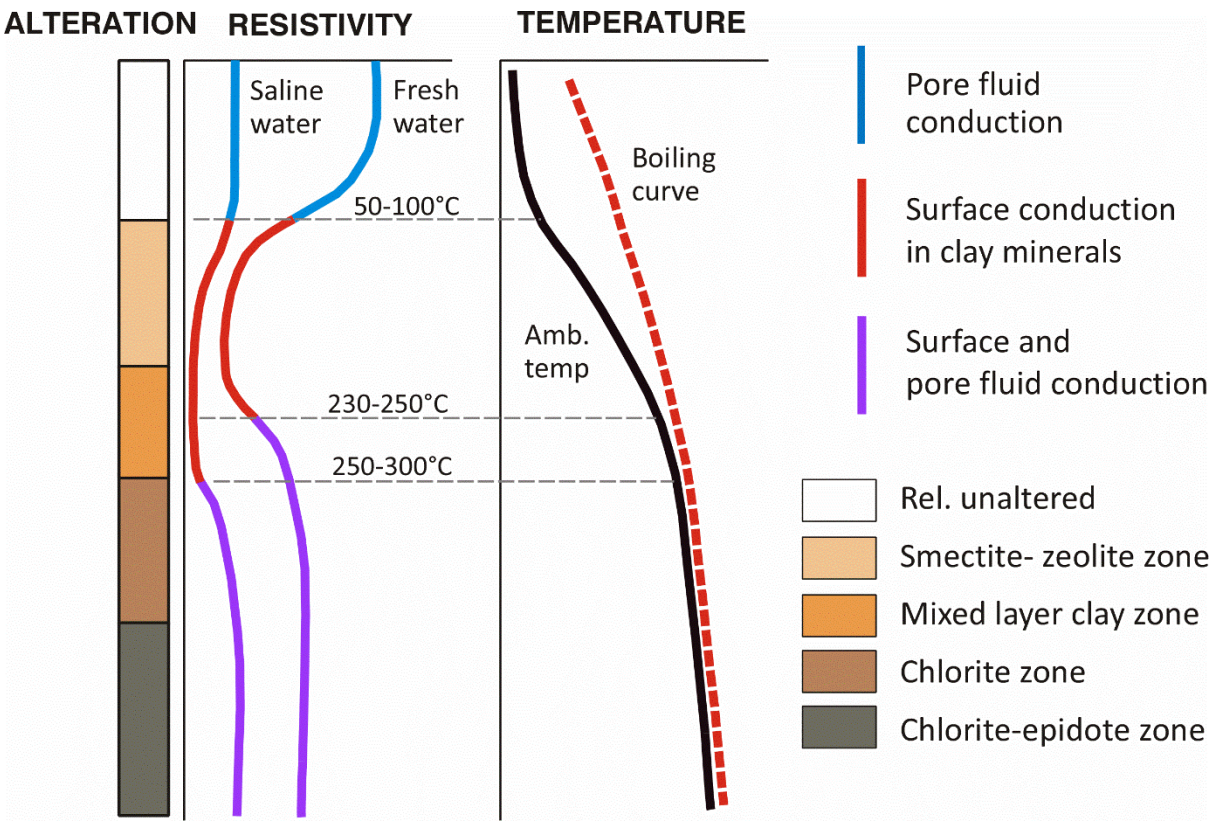

FIGURE 2: The general resistivity structure and alteration of the basaltic crust in high temperature areas summarized. Taken from Hersir et al., 2022

In the presence of water and sufficient temperatures, rocks undergo alteration and subsequently produce alteration minerals that are characteristic of the formation temperatures at that time (see Figure 2). The alteration minerals have characteristic resistivity signatures which can be imaged by the MT and TEM methods.

3.1. MT and TEM Data Acquisition

The TEM data reported were obtained using two types of equipment, i.e., the Zonge GDP 32^{24} and the Phoenix, V8 receiver and T4 transmitter.

For the Zonge equipment, a source loop of $15625m^2$ and a receiver loop of 10,000 m^2 were used. On the other hand, a 10,000 m^2 receiver and source loop were used for the Phoenix setup. Figure 3 shows the Phoenix V8 receiver and its T4 transmitter for TEM data acquisition.

MT data acquisition in the Buranga prospect was done using the five-component data acquisition (MTU-5A) instrumentation from Phoenix geophysics having three magnetic field channels i.e., the H_x, H_y, and H_z, two horizontal components of the electric field, E_x and E_y. The average electric dipole spacing was 80m and an average data collection duration of 18 hours.

FIGURE 3: The V8 receiver (a) and T4 Phoenix transmitter (b)

From all the data that were collected from this area, 75 TEM and 117 MT stations have been used in the 1D inversion presented in

this paper. Figure 4 shows the location of the MT and TEM data sites.

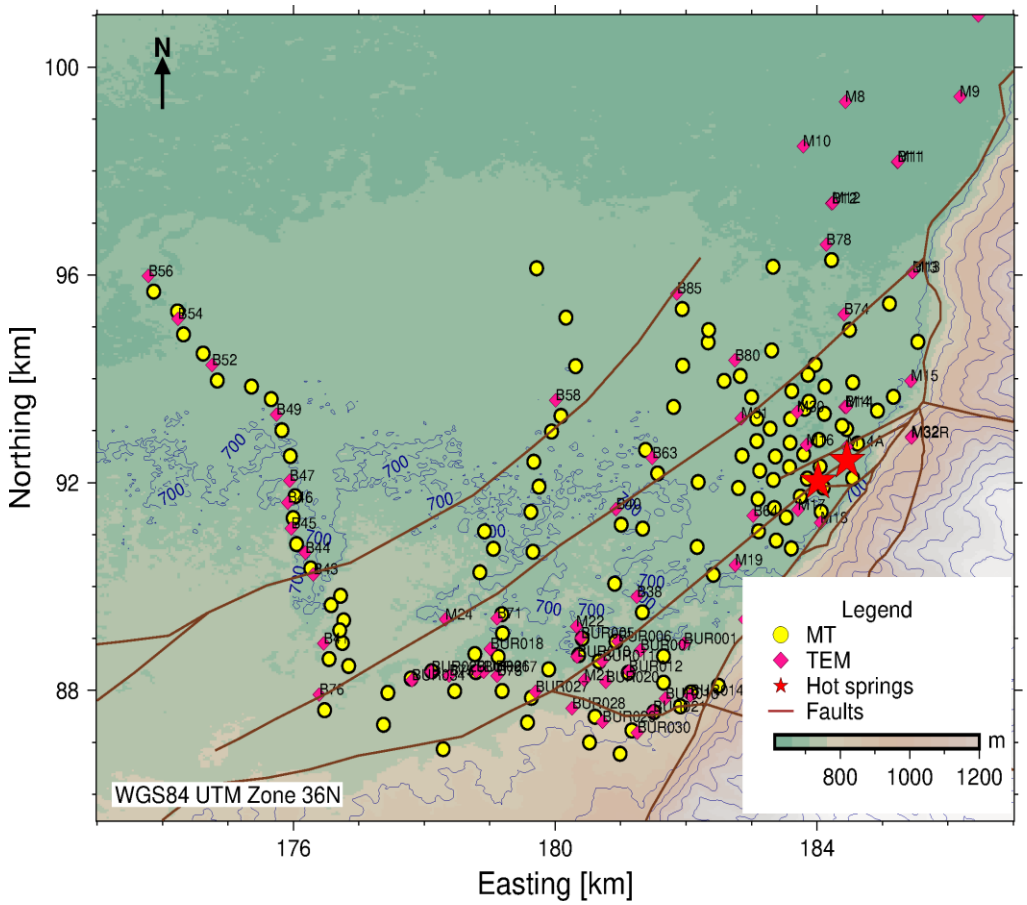

FIGURE 4: Location Map of the TEM (pink) and MT (yellow) soundings at Buranga prospect

4. DIMENSIONALITY AND STRIKE ANALYSIS OF MT DATA

Dimensionality analysis is critical in recognising 1D, 2D or 3D structures from modelling and inversion. The analysis method by Phase Tensor, PT (Caldwell et al., 2004) was applied in characterizing the dimensionality of local and regional subsurface structures because it is not affected by galvanic distortion. By studying phase tensor ellipses, we can obtain

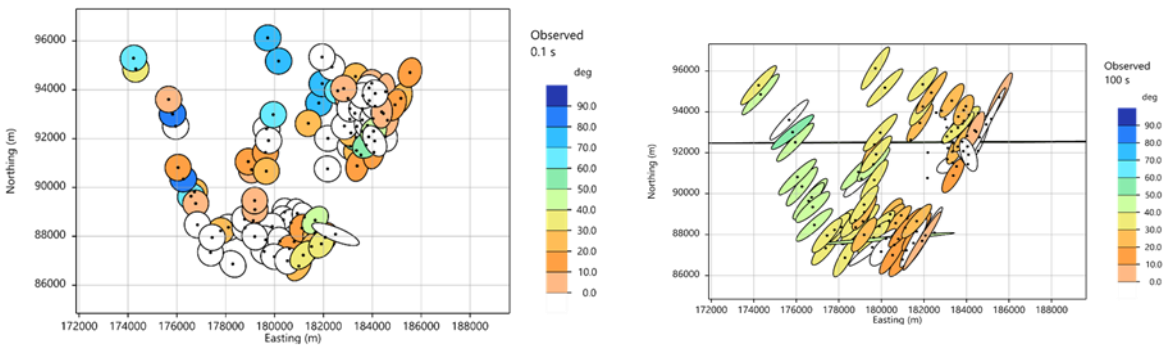

FIGURE 5 (a): Phase tensor ellipses at 0.1s and (b) Phase tensor ellipses at 100 s, coloured by angle β , the ellipses are aligned in a NE-SW direction. The black dots are the MT soundings (Coordinates are in UTM zone 36N)

information on dimensionality and horizontal resistivity variations or boundaries. For layered (1D) earth the phase tensor ellipses become circles, but in the case of 2D and 3D earth they are elongated in the electrical strike direction. The phase tensor analyses also estimate a skew angle β which is a measure of three-dimensionality (3D) of the resistivity structure.

Phase tensor ellipses are shown in Fig. 5a and Fig. 5b for the periods of 0.1s and 100s. They display the skew angle by a colour scale. For short periods (high frequencies>10 Hz), corresponding to shallow depths, low ellipticity (almost perfect circles) and skew values are observed within the area, attesting to a nearly 1D environment. At long periods (lower frequencies< 0.01 Hz), higher

dimensionality conditions (shown by perfect elipses) are observed, suggesting 2D or 3D environments. This indicates that at depth, there is a controlling strike in the area that is trending in the NE-SW direction

4.1 Tstrike and Zstrike

Electrical strike analysis of MT data indicates the directions of resistivity contrasts often due to geological structures, not necessarily seen on the surface. In addition to the resistivity structures below and around the site, the elements of the MT impedance tensor depend on the orientation of the x and y directions of the field layout, which in this case is N-S and E-W, respectively. For a 2D Earth, the resistivity varies with depth and in one of the two principal horizontal direction. The horizontal angle perpendicular to that direction is called the electrical strike. The angle it makes with geographical north is called Swift angle or Zstrike, Φ (Hersir et al., 2022).

By mathematically rotating the sounding data (by the Swift angle) to a coordinate system with either x- or y-axes parallel to strike direction, the off-diagonal elements of the impedance tensor become zero. Hence, the Swift angle has a 90° ambiguity. The depth of investigation increases with period and Zstrike depends on the period. The dominant electrical strike can be different at different depths, hence the Swift angle, or Zstrike can vary with period. Figure 6 shows Zstrike for periods 1–10 s.

Another parameter that is used to analyse directionality is the Tipper, **T**, which relates the vertical component of the magnetic field to the two horizontal components.

$$\boldsymbol{Hz = TxHx + TyHy}$$

Where T_x and T_y are the x and y components of the Tipper, respectively. For 1D earth the Tipper value is zero, i.e., $T_x = T_y = 0$. For a 2D Earth, the coordinate system can be rotated so that the x-axis is in the strike direction, the so-called Tstrike, that is, $T_x=0$, but $T_y \neq 0$. This is done by minimizing $|T_x|$. Unlike the Zstrike, Tstrike doesn't suffer the 90° ambiguity.

Strike analysis maps in Figure 6, at periods of 1-10 s show an alignment of a deep NE-SW controlling structure at the Buranga area

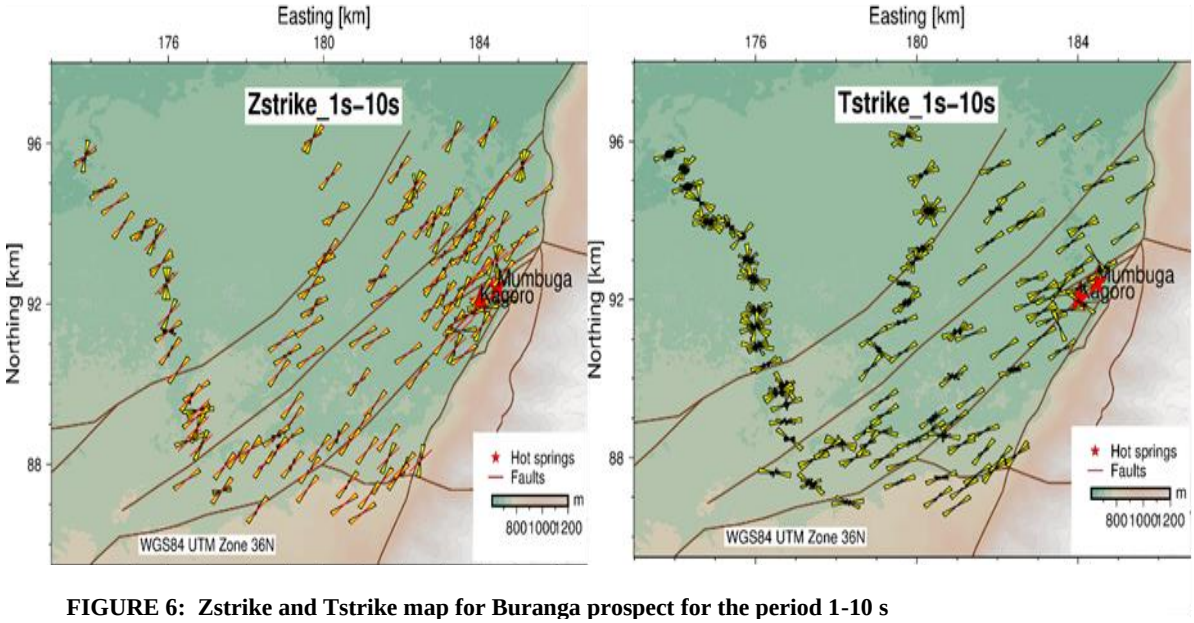

FIGURE 6: Zstrike and Tstrike map for Buranga prospect for the period 1-10 s

where we have the main controlling faults. This alignment agrees with the location of the surface manifestations which are found approximately along a line striking about N20°E, sub parallel to the local (Bwamba) fault. This indicates that the resistivity changes the least in the NE-SW direction but changes considerably perpendicular to the faults.

5. DATA INVERSION

For this paper, the TEM and MT data were inverted using the UNIX/LINUX based temtd program (Árnason, 2006) which is capable of performing both Occam and layered inversion. The temtd program can be used to jointly invert TEM and MT data or separately.

The inversion is based on the Levenberg-Marquardt nonlinear least square inversion. The misfit measure is the root mean square

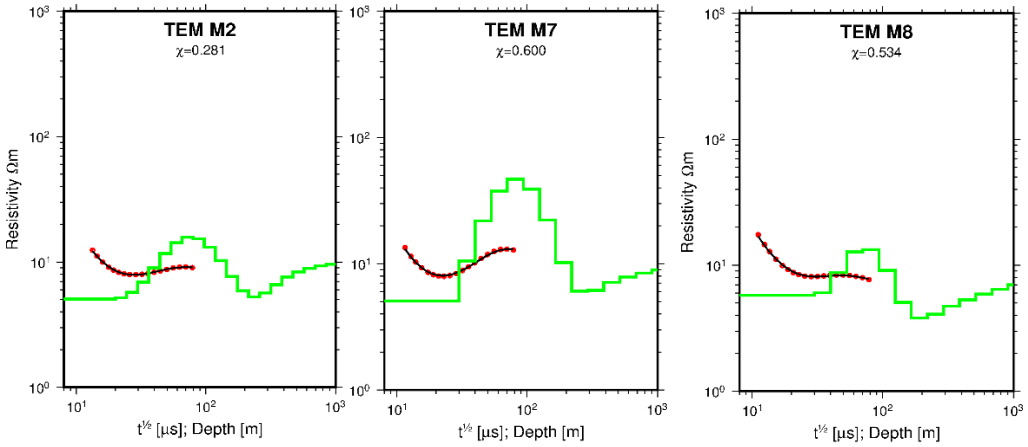

FIGURE 7: 1D inversion of three TEM soundings M2, M7 and M8 from the Buranga prospect. Red dots are the measured apparent resistivity values; the black line shows the calculated apparent resistivity based on the 1D model in green, χ is the RMS misfit between the measured and calculated data from the model.

difference between the measured and calculated values (chi square), weighted by the standard deviation of the measured value. Smooth models with respect to resistivity variations between layers and layer thicknesses can be achieved by using the damping factors which counteract sharp steps and oscillations in the model values.

MT suffers the so-called "static or telluric shift" due to local resistivity anomalies at or close to the sounding site. It distorts of the apparent resistivity by a multiplicative constant, S, and hence by a shift when presented on a log scale (Árnason, 2015).

The temtd program was used to jointly invert data from 63 MT stations with co-located TEM data. Joint inversion is important as it eliminates the effects of static shift. The rotationally invariant MT determinant apparent resistivity was inverted by (smooth) Occam inversion with the most appropriate model parameters until a reasonable fit between the TEM and the MT was obtained. Figure 8 shows two result of such joint inversion.

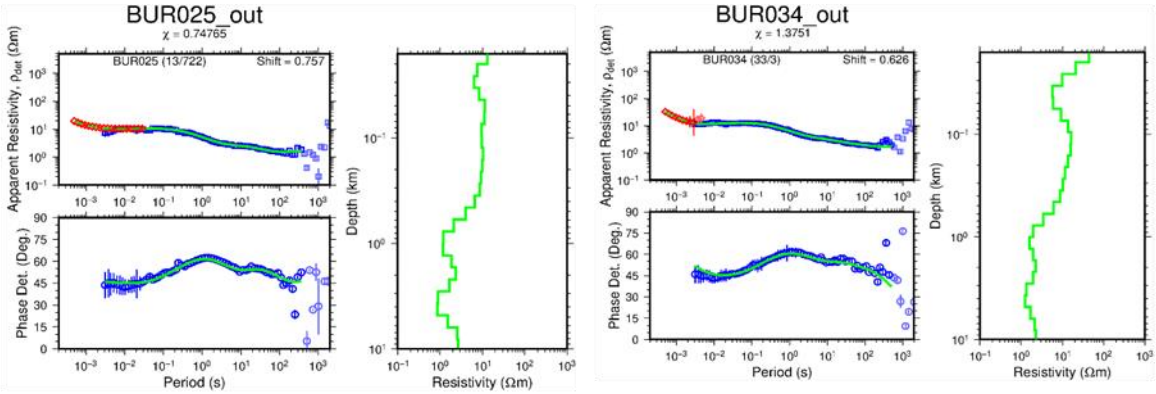

FIGURE 8: Results of joint inversion of two MT stations with two co-located central loop TEM soundings. The plot shows the measured TEM data (red diamonds) and Measured MT data: resistivity (blue squares) and phase (blue circles) together with the resultant inverted phase and apparent resistivity curves (solid green), a 1D Occam inversion model (right)

A histogram of static shift multiplier from joint inversion of MT and TEM data is shown in Figure 9. The observed shift at Buranga could be attributed to topographic effects towards the Rwenzori ranges that can cause telluric distortions (Didas and Hersir, 2020). By studying the spatial distribution of static shift at Buranga, it was noted that the MT soundings within the conductive sediments

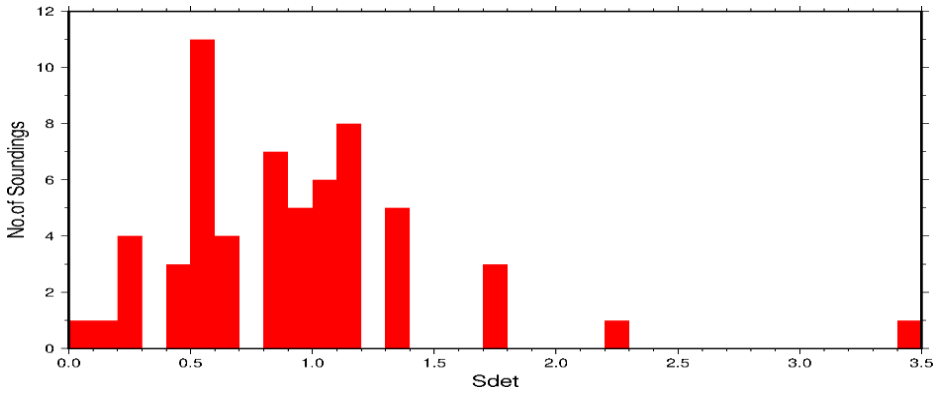

FIGURE 9: Static shift multiplier Histogram for Buranga

would not show much static shift. Therefore, in areas within the sediments where there were no available co-located TEM soundings, the MT data were inverted independent of the TEM data. It is, however, recommended by the authors to carry out infill TEM survey at locations with only MT stations to fully constrain the inversion and eliminate uncertainties due to static shift.

In addition to the 63 jointly inverted stations, 54 MT soundings were inverted as stand-alone MT data sets since there were no co-located TEM soundings at these locations (Figure 10).

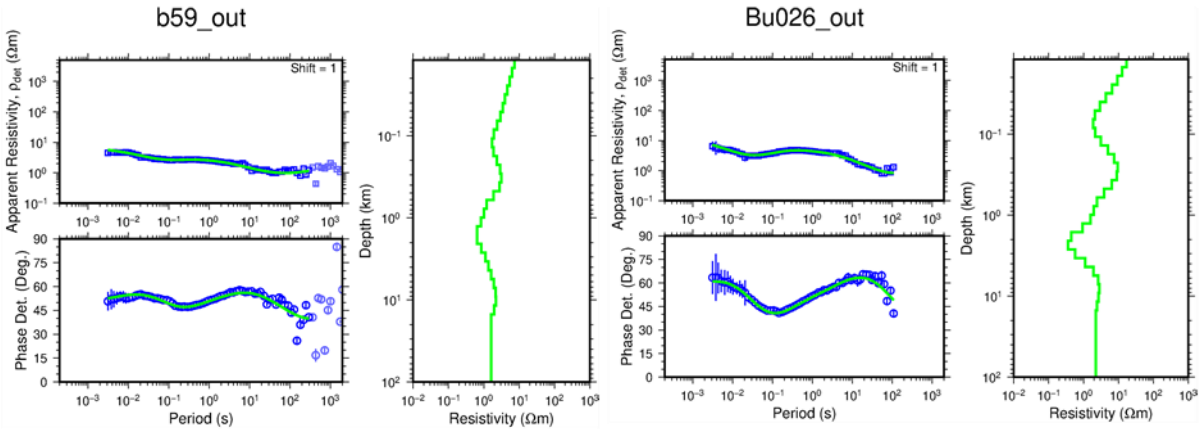

FIGURE 10: Example of the results from MT standalone inversion. Inversion outputs of apparent resistivity and phase curves are shown in green solid lines to the left while 1D resistivity depth models are shown in light green curves to the right. Measured resistivity and phase data are shown by blue squares and circles respectively to the left.

6. DISCUSSION OF THE RESULTS FROM THE INVERSION.

6.1 Resistivity depth slices

Depth resistivity slices were generated using the Temresd program developed at ÍSOR. The resistivity depth slices help us to understand the general lateral trend of the resistivity at different depths below the surface. Figure 12 and Figure 13 show four depth slices.

The resistivity depth map below at 600 m a.s.l (about 50-100 m below surface) shows a conductive zone of about 2-4 Ωm (marked in black stippled oval) around the hot springs and a resistive >10 Ωm towards the NE with a clearly defined and sharp boundary north of the surface manifestations which might be an indication of a contact zone probably due to a cross cutting fault (shown as black

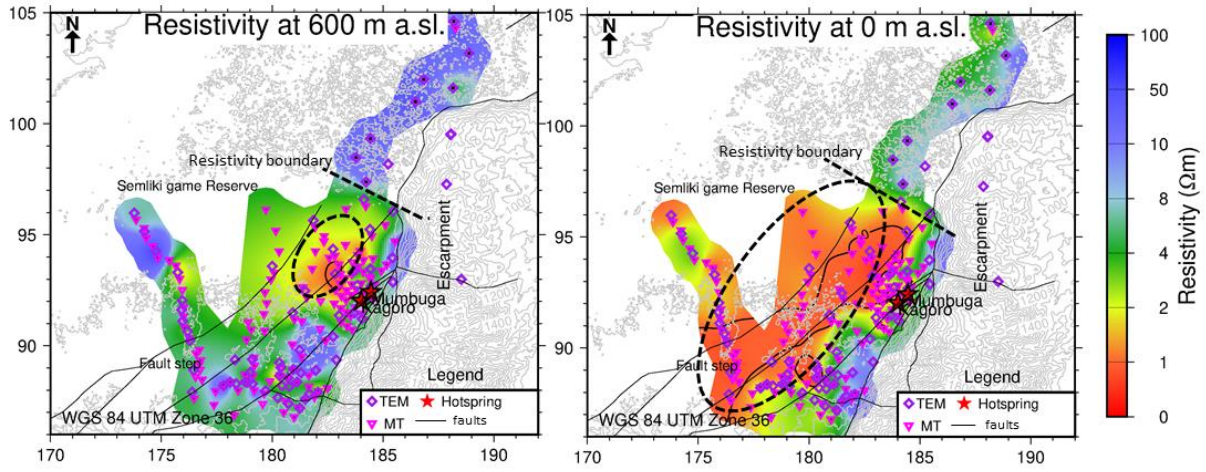

FIGURE 11: Resistivity depth slices at 600 m a.s.l (left) and 0 m b.s.l (right). Coordinates are UTM (zone 36) in km. Black dotted line represents a probable fault, and oval dotted conductive zones a resistivity boundary

stippled line) trending almost ESE-WNW. There is also a resistivity contrast of 8-10 Ωm on the far east (towards the Rwenzori massif) of the prospect.

At sea level (right in Figure 11), the conductive zone has increased in size, now covering most part at the centre of the prospect area, from at the border between the massif and in the sedimentary plain to the west. This could indicate conductive geothermal fluids within the sediments flowing west ward.

Figure 12 shows resistivity depth slices at 200 m b.s.l and 3000 m b.s.l.

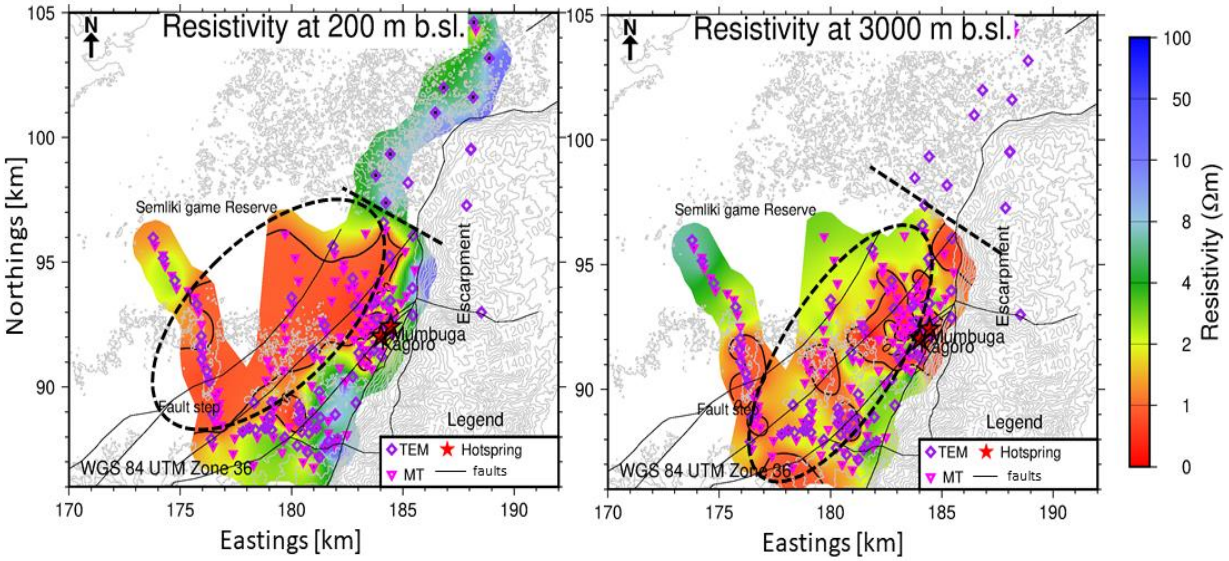

FIGURE 12: Resistivity depth slices at 200 m b.s.l (left) and 3000 m b.s.l (right). Coordinates are in km

The resistivity map at 200 m b.s.l (Figure 12, left) also outlines a conductive zone parallel and along the main faults in the area. This is probably due to the up flow of conductive geothermal fluid through the fault zones and flowing out into the sediments along and above the fault zone (damage zones or fault splays).

In the resistivity map at 200 m b.s.l (about 900 m below surface, Figure 12, left), the conductive zone, 1-2 Ωm becomes very pronounced and clearly demarcated, starting near the hot spring area and spreading out towards the west probably indicating an extensive area of thick conductive sediments which could as well indicate the out-flow zone of the system. Here, the lithology

boundary in the NE and on the eastern side is still maintained clearly showing the high resistive precambrian rocks of the mountain ranges and the conductive sedimentary basin in the graben.

Beyond 1200 m b.s.l, the resistivity boundary towards the NE disappears at this depth, the TEM stations to the NE of the prospect are not used in the plotting of the resistivity map. Because of the shallow depth of penetration of TEM soundings which is at most 1km. Therefore, at greater depths they have been ignored.

At 3000 m b.s.l, as shown on the right in Figure 12, the conductive zone starts to become thinner towards the centre around the hot springs. There is a relatively resistive zone that starts to show up at greater depths probably indicating a gradual change from the conductive sediments into a more resistive unit at depth. The depth to basement at Buranga is not known, but a few km north of the geothermal field, the bottom of sediments was determined to be at 5000 m b.s.l from oil and gas wells.

6.2 Resistivity cross sections

A number of vertical resistivity cross sections were constructed as shown in Figure13. The cross sections were generated using the temcross program which is a Linux based code developed at ÍS

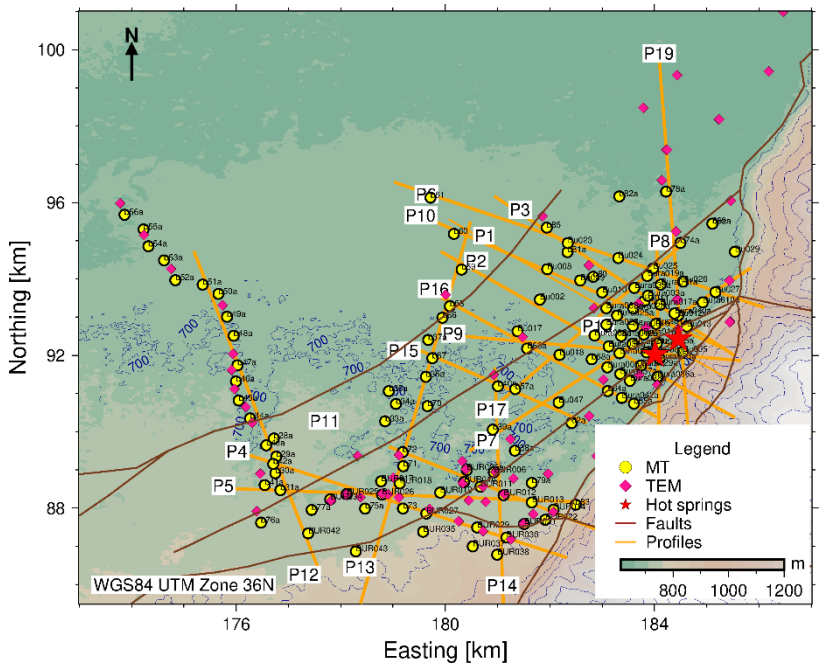

FIGURE 13: Location of the resistivity cross sections

Profile 1

Profile 1 (Figure 14) runs NW-SE and passes close to the Mumbuga hot spring area (see Figure 13). Two

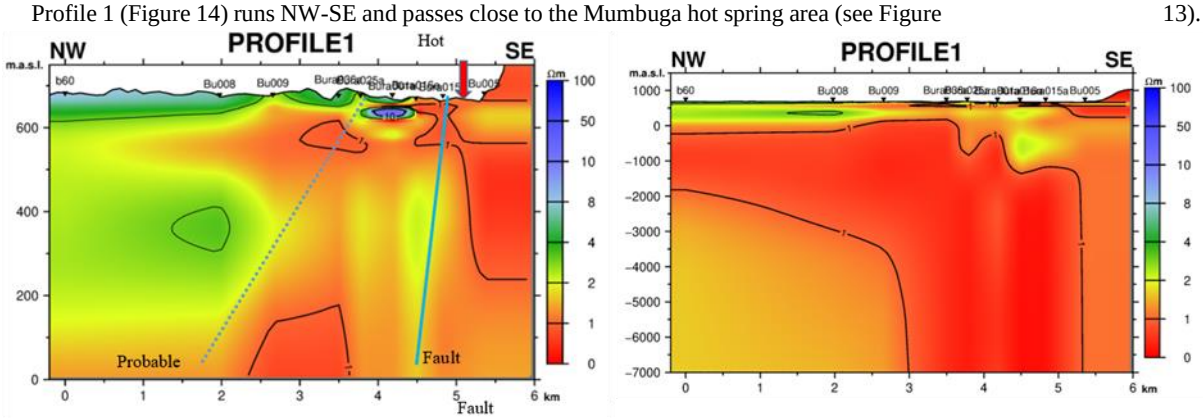

FIGURE 14: Resistivity cross section down to sea level, (left) and down to 7000 m b.s.l (right). For location see Figure 13.

sections reaching different depths were generated with one from surface to sea level and the other from surface down to 7 km b.s.l. In the section on the left, a top layer of 2-8 Ωm is seen extending to a depth of 200 m b.s.l. It is underlain by a thick more conductive

layer extending to more than 5000 m b.s.l. The more conductive parts of the section could probably be pointing at thick sedimentary layers (alluvial soils) that have filled up the graben over time.

Profile 2

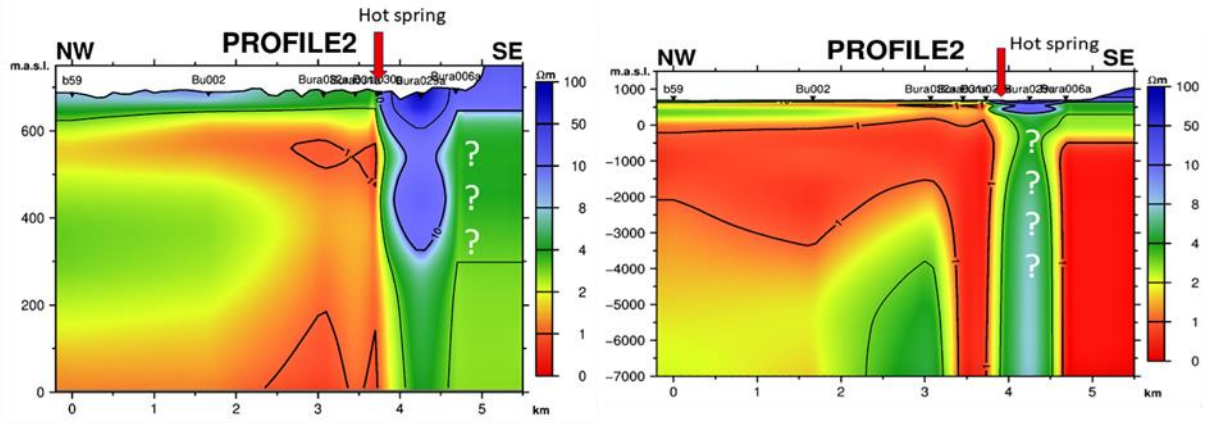

FIGURE 15: Resistivity cross section along profile 2. The question marks indicate an area of unreliable data from one station. The hot spring is located along the inferred fault. For location, see Figure 13

Profile 2, (Figure 15), also runs NW-SE through the prospect area and passes slightly the southern part of the Kagoro hot springs (see Figure 13). At shallow depths on the SE part of the profile, there exists a resistive Precambrian rock typical of the Rwenzori massif with resistivity >50 Ωm. In the NW part of the section, there is a layer 3-7 Ωm and about 100 m thick over lying more conductive thick sedimentary layers that extend to depths of almost 4 km.

The model from station Bura029a stands out, probably due to bad/ affected sounding data. This station alone cannot be relied on to give a conclusive resistivity structure since the inferred resistivity at that station is not imaged by nearby stations as seen in Figure 16.

Profile 6

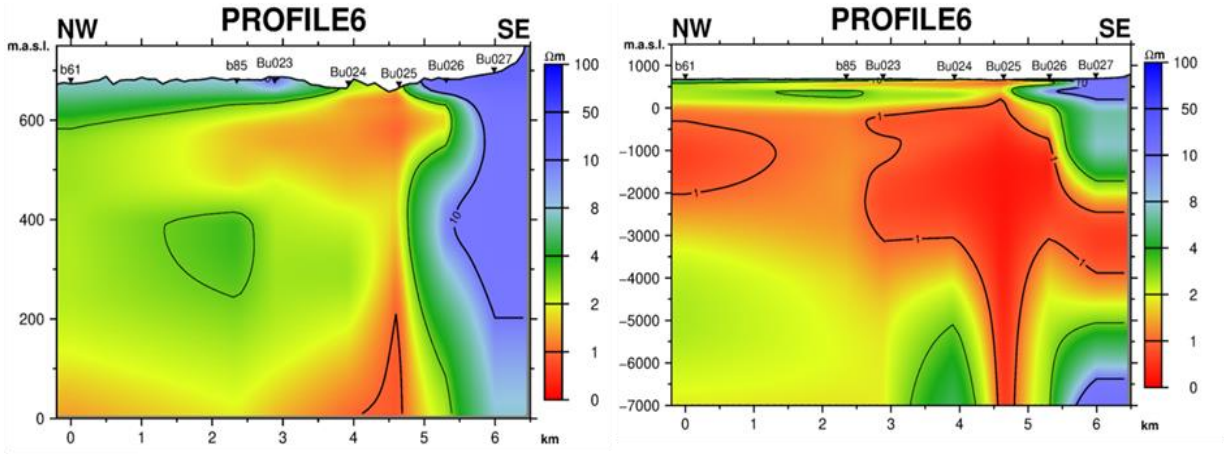

FIGURE 16: Resistivity cross section on profile 6 NW-SE based on 1D joint inversion of MT and TEM data at Buranga down to 7km. For location see Figure 13

Cross section from profile 6 (Figure 16) is a NW SE trending profile (see Figure 13) starting from the high resistive Precambrian rocks of the host block in the SE at the near surface towards the more conductive sediments as you move towards the NW. There is a low resistivity layer, at about 700 m below the surface, with a thickness of about 3km on the most North westerly side. This low restive cap is underlain by a relatively resistive layer from 4km b.s.l onwards.

Profile 9

Profile 9 (Figure 17) trends from the west to the east of the Buranga prospect crossing the Kagoro hot spring area and also crossing the faults inferred by geological mapping (see Figure 13). The section shows a relatively resistive surface layer of about 2-5 Ωm and 100 m thick from the western side towards the centre and on the far eastern end. At the centre, there is a more conductive layer extending to the surface making a doming shape around a deep seated more resistive body at 2 km below sea level. This resistive

zone (the right in Figure 17) could be an artifact due to poor-quality data since this structure cannot be seen in any of the other soundings. Data at this sounding should be re-acquired to eliminate any doubts.

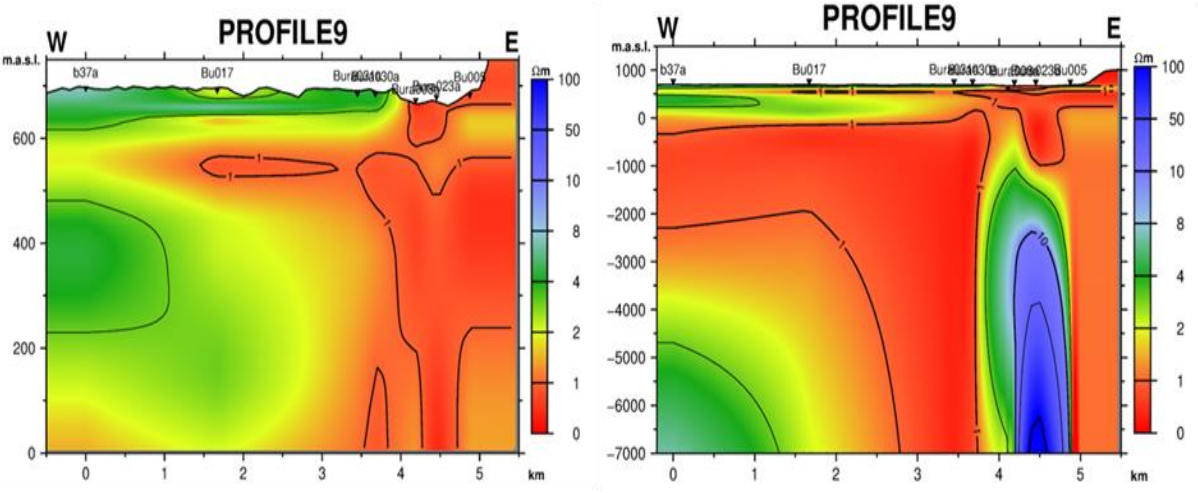

FIGURE 17: Resistivity Cross section on profile 9, W-E down to 7km. For location see Figure 13.

Profile 19

Cross section 19 (Figure 18) runs from the mid -southern part of the prospect area to the northern side of the area at Buranga (see Figure 13). This profile was constructed to investigate the resistivity boundary that was observed on the iso resistivity maps towards the North-eastern side of the survey area. From the section, the following can be observed:

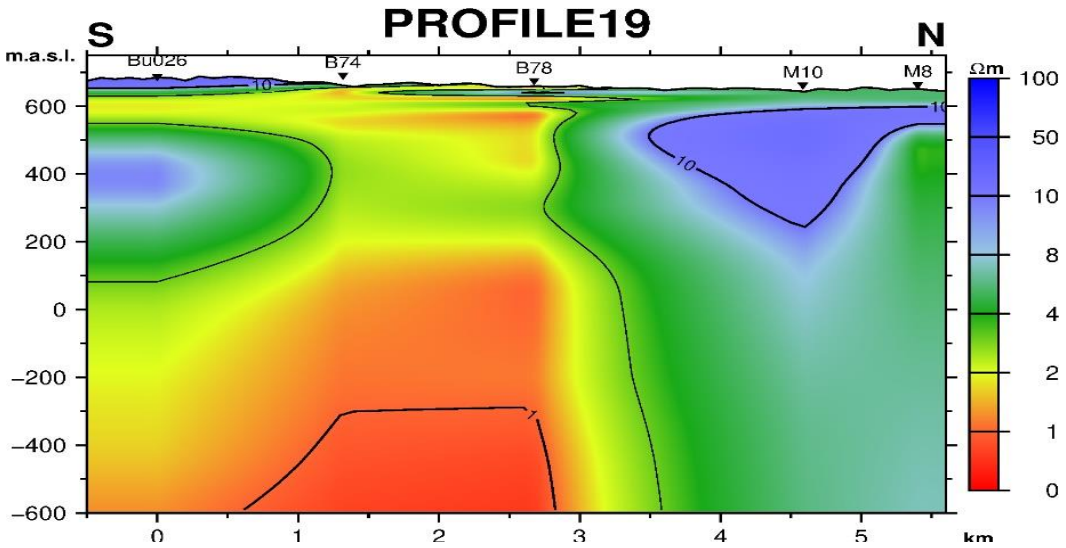

FIGURE 18: Resistivity cross section 19 S-N based on 1D joint inversion of MT and TEM down to 600 m b.s.l. For location, see Figure 13.

(a) Indeed, there exists a clear resistivity boundary near station B78. it is less resistive to the south and more resistive in the north. This resistivity boundary could represent a contact zone or a W-E cutting fault dipping to the north and is concealed by the vegetation in the area.

(b) South of B78 is dominated by conductive alluvial soils (rift alluvium) or sediments with resistivity < 4 Ωm whereas north of B78 are probably the so-called mica schists and quarzitic interbeds with resistivity > 5 Ωm.

6.3 Geothermal significancy of results and Integrated interpretation

The resistivity structure at Buranga can be described as follows:

(a) From near surface down to 400 m a.sl.

From surface to a depth of about 200 m, the area is characterized by relatively resistive layers ranging from 8 Ωm on the western side to over 100 Ωm to the east towards the Rwenzori ranges. This corresponds to unaltered surface impermeable rocks to the east and to

soil assemblages that have recently been deposited on the western side in the flood plain where there is constant deposition of surface soils from the Rwenzori.

(b) Below 400 m a.s.l to about 4km bl.sl.

There are thick conductive sedimentary layer (s) (approximately 4km thick with resistivity <5 Ωm) from near the hot spring area and spreading out towards the west with the hot springs being on the east most part. This low resistive layer could be due to up flow of geothermal fluids into the sediments along the main fault(s) and then flowing within the sediments towards the west.

(c) Below 4 km.

The thick conductive sediments extend to a depth of 4km and after that they are underlain by a layer of 4-8 Ωm in the western part. This indicates that the depth to crystalline basement west of Buranga could be at 5 km. There is a clear contrast in the eastern most part with resistivities of > 50 Ωm. This is probably the basement rocks towards the Rwenzori. The resistivity boundary to the west and east at MT station Bu026 in cross section 19 (Figure 18) could infer a deep-seated fault. This fault could be the pathway for deep circulating hot fluids to the surface at the hot springs above.

Geochemical and isotope hydrological studies by Bahati et al., (2010) show that the fluids from the hot springs and hot pools at Nyansimbe and Kagoro are neutral with a PH of 7-8 and salinity of 14,000 – 17,000 mg/kg total dissolved solids. The conductivity of the fluids can explain the high conductivity (low resistivity) that is seen within the sediments. Geothermometry predicts subsurface temperatures of about 180°C and no indication of hydrogen was found in gas analysis, (Bahati et al., 2010) and there are no indications of mixing of the geothermal and cold ground water.

7. CONCLUSION AND RECOMMENDATIONS

The resistivity data in this study support previous ideas about Buranga geothermal system. It is a deep circulation in boundary extracting heat from the general crustal heat flow and thus no volcanic heat source.

The actual resistivity structure in the eastern part, in the vicinity of the controlling faults, is somewhat ambiguous due to poor data quality.

Up flow is mainly controlled by the main Bwamba bounding fault(s) where the permeability is within the damage zone and fault splays directly associated with the N to NE striking west dipping faults as mapped by Hinz et al. (2018). Based on the distribution of active hot springs, the up flow is probably along multiple fault segments.

The area has a very thick layer of sediments about 5km deep in the central rift north of Buranga. The geothermal system has an outflow into these sediments and towards the western part of the surveyed area. Recharge is by meteoric water (Ármannsson, 1994 in Bahati et al., 2010) that runs from the Rwenzori ranges into the flood plain within the area and then seeping through smaller fault terminations and displacement transfer zones that are present within this young faulting system. There was no high resistivity core detected at depth and no high temperature alteration detected. Estimated subsurface temperatures are slightly above 150°C. Smectite clays are the most probable alteration minerals to be expected in this area.

Therefore, as a recommendation, higher quality resistivity data should be collected in the eastern part to better resolve the resistivity structure there. Gravity survey should be undertaken on profiles running from the Rwenzori into the sedimentary basin together with local scale reflection/refraction seismics to map the topography of the basement a well as passive micro-seismic monitoring. If there might exist such data from previous studies, they should be reviewed and used to constrain the current model.

When the current model has been improved by obtaining better quality resistivity data, gravity, and (or) seismic data, then drilling temperature gradient holes and/or an exploration well should be considered. Drilling of an exploration well would target the deep permeable fault zones which provide the up flow. Temperature gradient holes could help locating the up-flow fault(s) and define the extent of the geothermal system.

8. ACKNOWLEDGEMENT

The first author acknowledges the support of the GRÓ-Geothermal Training Program for the six months training in 2021 in Iceland during when most of the data analysis and interpretation was done.

The first author would also like to thank the leadership at the Directorate of Geological Survey and Mines (DGSM) for providing the resources to acquire the data and also allowing the authors to use the data in this study.

9.REFRENCES

Árnason, K., 2015: The static shift problem in MT soundings. In: Proceedings of the World Geothermal Congress 2015, Melbourne, Australia, 12 pp.

Árnason, K., 2006: temtd, a program for 1D inversion of central-loop TEM and MT data. ÍSOR – Iceland GeoSurvey, a short unpubl. manual, 17 pp.

Bahati, G., Kato, V. and Nyakecho, C., 2010: Geochemistry of Katwe-Kikorongo, Buranga and Kibiro Geothermal Areas, Uganda. Presented at the 3rd east African Rift geothermal conference (ARGEO-C3) Djibouti, 22 – 25 November 2010

Didas, M.M. and Hersir, G.P., 2020: 1D joint inversion of MT and TEM data from Ngozi geothermal prospect, southwest Tanzania. An integrated interpretation of geoscientific results. Proceedings of the World Geothermal Congress 2020+1. Reykjavik, Iceland.

Caldwell, T.G., Bibby, H.M. and Brown, C. 2004: The Magnetotelluric phase Tensor, In Geophysical Journals International. (2004) 158, 457–469.

Heath, J., Sussman, D., Lonsdale, A. and Bayarsaikhan, M., 2018: Advancing Geothermal Development in East Africa: Lessons Learned During the 2015-2018 EAGER Programme. In: Proceedings of the 7th African Rift Geothermal Conference 2018. Kigali, Rwanda. P13.

Hersir, G.P. Árnason, K., 2009: Resistivity of Rocks. Presented at "Short Course on Surface Exploration for Geothermal Resources", organized by UNU-GTP and LaGeo, in Ahuachapan and Santa Tecla, El Salvador, 17-30 October 2009.

Hersir, G.P., Gudnason, E.Á., and Flóvenz, Ó.G., 2022: Geophysical exploration techniques. In: Letcher, T.M (eds.) Comprehensive Renewable Energy – 2nd edition, Vol 7, pp.26-79. Oxford: Elsevier, http://dx.doi.org/10.1016/B978-0-12-819727-1.00128-X.

Hinz, N.H., Mark, C., Faulds, J.E., 2016: Regional Quantitative Play Fairway Analysis: Methodology Global Examples and Application For The East African Rift System. In Proceedings, 6th African Rift Geothermal Conference Addis Ababa, Ethiopia, 2nd – 4th November 2016.

Kahwa, E., Nishijima, J. and Fujimitsu, Y., 2020: Subsurface Characterization of Panyimur Geothermal Prospect, NW Uganda using Magnetotelluric Data. In: Proceedings of the 8th African Rift Geothermal Conference Nairobi, Kenya: 2 – 8 November 2020

Lindenfeld, M., Rumpker, G., Batte, A., Schumann., 2012: Seismicity from February 2006 to September 2007 at the Rwenzori Mountains, East African Rift: earthquake distribution, magnitudes and source mechanisms: In Solid Earth · August 2012 DOI: 10.5194/se-3-251-2012

Morley, C.K., and Westcott, W.A., 1999: Sedimentary Environments and Geometry of Sedimentary bodies determined from Subsurface Studies in East Africa. In: Morley, C.K. ed., Geoscience of Rift Systems-Evolution of East Africa. AAPG Studies in Geology 44, 211 - 231.

Natukunda, J, F., 2010: Geology of Kibiro, Katwe and Buranga Geothermal Prospects of Uganda. In: Proceedings of the World Geothermal Congress 2010 Bali, Indonesia, 25-29 April 2010.

Nyaketcho, C., 2008: Preliminary Environmental Impact Assessment for the Development of Buranga geothermal prospect, Uganda Report 26 In: Geothermal Training in Iceland 2008. UNU-GTP, Iceland, 447-476.